SUPPLEMENTAL MATERIALS

S1. Scale up from 10 nL chip-based FID Crystallization Screens

The screening of various kinetic trajectories was tested by exporting successful nanoliter-volume μFID crystallization conditions to 125 nL reactors on the optimization chip. The osmotic bath and permeation barrier protocols were evaluated in scaling up the crystallization of a total of 14 targets including 8 well-characterized crystallization standards (chicken egg white lysosyme (LYS), ferritin (FER), glucose isomerase (GI), bovine liver catalase (CAT), recombinant human insulin (INS), xylanase (XYL), alphalactalbumin (ALPH), and thaumatin (THM), three previously crystallized integral membrane proteins (the mechanosensitive ion channel of large conductance (MSCL) from *E. coli*, bacteriorhodopsin from the archeaon *Halobacterium* NRC-1 (BOP), and a BOP point mutant (BOP D85S)), one nucleic acid/protein complex known to require precise crystallization conditions in hanging drop (the *E. coli* Rho transcription termination factor with $r(CU)_4$ RNA and AMPPNP (Rho)), and two targets of unknown structure that had been crystallized only in μFID format (the transferrin receptor heterodimer complexed with HFE (hdTFR/HFE), and a mutant P450 alkane hydroxylase (BM3 1-12G)). In all trials, protein samples were equilibrated by free interface diffusion against a successful crystallization agent whose identity was determined by prior μFID screening on chip. Simultaneously, the rate and extent of vapor transport were screened across the twenty reactors by varying the concentration of the osmotic bath solution or the thickness of permeable oil layer.

The permeation barrier protocol was successful in improving crystal morphology and increasing crystal size for of all 14 targets tested. This success, which occurred despite the highly varied sample pool, establishes this approach as a high correspondence method for scaling up nanoliter volume crystallization. In contrast, the osmotic bath protocol was successful in scaling up crystallization conditions for only five of the ten targets, including all eight model proteins, BOP, BOP D85S, and MSCL. In particular, multiple subsequent trials using hdTFR/HFE, Rho and P450 1-12G failed to produce crystals despite extensive screening of the final reaction state. This lack of correspondence may be due either to insufficient concentration of the osmotic bath solutions or to transient osmotic differences between the sample and the reagent wells, leading to unwanted convection between the wells. In the later case this behavior can be avoided by using a permeation barrier protocol during the transient FID stage, followed by an osmotic bath protocol for longer times.

S2. Crystal Growth Conditions

Crystals of ferritin (type 1 from horse spleen; Sigma Aldrich Company) were grown by FID diffusion at 4 °C of 2 parts protein stock (34 mg/mL ferritin, 150 mM sodium chloride) against 1 part crystallization agent (1 M sodium acetate, 50 mM cadmium sulfate, 100 mM HEPES·HCl, pH 7.5) with an osmotic bath solution consisting of 50 % crystallization agent. Crystals of insulin (human recombinant; Sigma Aldrich Company) were grown by FID diffusion at 25 °C of 1 part protein stock (10 mg/mL insulin, 25 mM HEPES·HCl, pH 8.2) against 1 part crystallization agent (30% v/v MPD, 200 mM magnesium acetate, 100 mM sodium cacodylate, pH 6.5) with an osmotic bath solution of 75% crystallization agent. Crystals of lysozyme (chicken egg white; Sigma Aldrich

Company) were grown by FID diffusion at 25 °C of 2 parts protein stock (85 mg/mL lysozyme, 100 mM sodium chloride, 100 mM sodium acetate, pH 4.5) against 1 part crystallization agent (4 M sodium chloride, 100 mM sodium acetate pH 5.2) with a reservoir solution of 140 μL of fluorinated silicone oil (poly-3,3,3-Trifluoropropyl-methylsiloxane; Hampton Research). Crystals of catalase (bovine liver; Sigma Aldrich Company) were grown by counter diffusion of 1 part protein stock (15 mg/mL catalase) against 1 part crystallization agent (25% v/v PEG 2000 MME, 100 mM potassium sulfate, 100 mM TRIS·HCl pH 8.5) over a period of 7 days with varying connecting channel lengths and osmotic bath strengths (% of crystallization agent).

S3. In Situ Diffraction Studies

A. Harvesting crystals for *in situ* diffraction studies

Sections of elastomer membrane containing protein crystals were excised from the chip and mounted for diffraction studies *in situ* both at room and cryogenic temperatures. For room temperature mounts, a 3/8" punch tool (Technical Innovations; Brazoria, TX) was inserted through the open face of the reagent reservoirs and used to cut around the periphery of the membrane, creating a thin PDMS disk containing the protein crystals. Membranes were harvested from selected reactors without disturbing adjacent reactions. Disks were sectioned into 1 mm thick strips and mounted on a standard magnetic "crystal cap" (Hampton Research; Aliso Viejo, CA) fitted with a small alligator clip as shown in Figure 3a of main text. In cases where the screening of a large number of crystals grown from identical conditions was desired the entire crystal disk was mounted without sectioning (Figure S1a). For diffraction studies at cryogenic temperatures, a variety of cryoprotectant

solutions were slowly introduced to the microwells containing crystals by diffusion across the connecting microchannel. At each reaction site the osmotic bath solution was replaced with a solution containing the appropriate concentration of crystallization agent and a cryo-protectant. The membrane covering microwell opposite to the crystals was then perforated using a microknife (Hampton Research), and the cryoprotectant was allowed to slowly diffuse into the crystal wells over a period of 1 to 3 days. Sections of membrane containing crystals were then harvested as described above and frozen by immersion in liquid nitrogen.

B. Crystal Alignment

Sections of PDMS membrane containing protein crystals were excised using a punch and mounted using standard crystal caps (Hampton Research) fitted with a 1 cm long alligator clip (Figure S1a). In addition to providing minimal x-ray attenuation, the short optical path through the PDMS membrane facilitates crystal alignment without significant errors due to optical aberrations or parallax despite the high index contrast ($n_{PDMS} = 1.4$). The excellent optical properties of the PDMS membrane are demonstrated in Figure S1b which shows the localized bleaching of a crystal of BOP precisely aligned to a pre-focused X-ray beam having a diameter of 30 microns.

C. *In Situ* Cryogenic Freezing

Suppressing microcrystalline ice formation requires rapid freezing so that vitrification occurs and nucleation is prevented. Despite the high surface to volume ratio and low thermal mass (~ 0.75 mJ / K) of the PDMS membrane strips, we were concerned that the

low thermal conductivity of the polymer (0.15 W / m K) may adversely affect freezing. To investigate this possibility, we measured the minimum concentration of cryoprotectant necessary for freezing a solution so as to form an amorphous glass. Diffraction patterns of frozen PDMS membranes filled with varying concentrations of glycerol ranging from 20 to 40 % (v/v) were analyzed to determine the minimum concentration required to suppress the formation of microcrystalline ice in frozen PDMS membranes. A sharp transition from a pronounced ice ring (top of Figure S1d) to a diffuse solvent ring (bottom of Figure S1d) was observed between 28 % and 30 % glycerol, corresponding to a minimum concentration of 29 ± 1 %. This value is very close to the minimum concentration of 27 ± 1 % determined for vitreous flash-freezing in a conventional 200 micron diameter nylon loop, indicating that heat transfer through the PDMS membranes is efficient.

D. Room Temperature Studies

Chip-grown crystals of lysozyme and MSCL were harvested for diffraction studies *in situ* at room temperature as described (methods). In this format the PDMS membrane protects crystals from the ambient conditions, avoiding rapid dehydration. Crystals of MSCL harvested by this method were stable for over an hour and showed no signs of deterioration, providing ample time for preliminary analysis on a home X-ray source. Room temperature diffraction studies were performed using a Rigaku RU200 generator and R-AXIS IV detector. One degree oscillation frames of lysozyme crystals taken at normal incidence through 250 μm PDMS disks, showed strong reflections to approximately 1.6 Å (Figure S1c), which was the limit of our detector. In addition to the usual solvent ring at 3.5 – 3.8 Å, diffuse scatter from the PDMS was visible as a powder ring at approximately 7

Å (Figure S1d, bottom). MSCL crystals diffracted much more weakly, with the highest angle reflections visible at approximately 12 Å. This weak diffraction was consistent with that obtained from crystals that were mounted and frozen in standard cryo-loops. The low resolution diffraction from MSCL crystals grown in this condition was used to quickly reveal the poor order intrinsic to this crystal form under native conditions and eliminated the need to attempt further optimization of freezing conditions.

E. X-ray Absorption of PDMS Membranes

The linear absorption coefficient of PDMS at X-ray energies of 8.05 KeV (corresponding to the Cu-α line) is approximately $\mu = 24.4\ cm^{-1}$ which is slightly less than that of borosilicate glass ($\mu = 30.0\ cm^{-1}$). For a 50 μm thick membrane this corresponds to a transmission factor of approximately 88%. At 11 KeV, an energy commonly used at synchrotron sources, the linear absorption coefficient of PDMS is reduced to approximately $7\ cm^{-1}$, corresponding to a transmission coefficient of approximately 97% for a 50 μm membrane.

The rectangular cross-section of the PDMS membranes results anisotropic X-ray absorption and background scatter during data collection (Figure S2a). This increased background scatter and attenuation due to the PDMS does affect the signal-to-noise ratio of the data as a function of membrane angle (Figure S2b). The mean I/σ passes through a minimum at approximately 80° due to the finite width and rectangular shape of the membrane, reducing the signal to noise by a factor of approximately three. We estimate that useful diffraction

data may be collected from crystals grown in the current format over an angle of 120°, which is sufficient for data collection on all but triclinic and monoclinic space groups.

F. Data collection, structure determination, and refinement

Data were collected at Beamline 12.3.1 at the Advanced Light Source [1] and processed using ELVES [2] and DENZO/SCALEPACK [3]. All MR solutions were built and refined using hands-off, fully automated procedures. Greater than 94% of the residues were correctly placed in all four structures and refined to an R-free value of 23% or without manual rebuilding (Supplemental Table 1). Molecular replacement (MR) was performed with Phaser [4,5] using poly-alanine or poly-glycine models generated from the following starting models: 1HEQ (lysozyme) [6], 1KWN (thaumatin) [7], 1CAT (catalase) [8], 6XIA (glucose isomerase) [9]. MR solutions were subjected to 8 rounds of fully automated protein model building and structure refinement using ARP/wARP [10] and REFMAC5 [11]. Electron density maps and refined models were inspected in O [12].

S4. In Situ Diffraction Data and Phasing Statistics

Table 1. Data collection and phasing and refinement statistics for diffraction studies *in situ*.

Crystallographic and Refinement Statistics					
	Lysozyme	**Thaumatin**	**Catalase**	**Glucose Isomerase**	**Thaumatin (home source)**
A. *Data Collection*					
Space Group	$P4_32_12$	$P4_12_12$	$P3_221$	I222	$P4_12_12$
Resolution (Å)	50 – 1.2	50 – 1.25	50 – 1.9	50 – 1.3	50 - 1.7
Unit Cell					
A (Å)	78.9	57.7	139.4	102.6	57.8
b (Å)	78.9	57.7	139.4	93.0	57.8
C (Å)	36.9	148.8	97.4	98.0	150.3
α β γ (°)	90 90 90	90 90 90	90 90 120	90 90 90	90 90 90
X-ray source	ALS 12.3.1	ALS 12.3.1	ALS 12.3.1	ALS 12.3.1	RAXIS-IV
Wavelength (Å)	1.13	1.127	1.127	1.116	1.542
Data collected (°)	60	80	30	100	47
Total reflections	191974	336451	218595	783377	363748
Unique reflections	36938	68255	86050	111486	26212
Multiplicity	4.7	3.2	2.5	3.7	3.2
Completeness (%)	84.8 (76.3)	91.5 (92.4)	70.3 (59)	97 (82.3)	90.6(43)
Wilson B-factor	10	12	18	13	20
Mosaicity (°)	0.08	0.06	0.1	0.2	0.5
R_{sym} (%)	4.7 (22.6)	6.6 (40.2)	6.9 (34)	8.2 (39.7)	4.2(20.1)
I/σ	9.6 (2.8)	2.4 (1.4)	8.7 (2.0)	3.6 (1.8)	23.3(2.1)
Crystal Volume (μm^3 x 1000)	3375	6000	640	1720	12000
B. *Phasing & Refinement*					
MR search model	1HEQ-polyG	1KWN-polyA	1CAT-polyG	6XIA-polyA	1KWN-polyG
MR program	Phaser	Phaser	Phaser	Phaser	Phaser
8 rounds of ARP/wARP auto building with subsequent REFMAC5 refinement					
Residues built	121/129	197/207	970/1012	384/387	200/207
Observation to Parameter ratio	6.16	8.86	1.87	8.71	3.87
R_{cryst} (%)	20.8	20.5	21.3	19.1	19.8
R_{free} (%)	23.9	23.0	28.6	21.0	22.9

[a] $R_{sym} = \Sigma_{hkl}|I(hkl)-\langle I(hkl)\rangle|/\Sigma\langle I(hkl)\rangle$, where $I(hkl)$ and $\langle I(hkl)\rangle$ are the measured and average intensities of multiple measurements of the same reflection.

[b] R_{cryst} (R_{free}) $= \Sigma_{hkl}||F_{obs}(hkl)|-|F_{calc}(hkl)||/\Sigma|F_{obs}(hkl)|$, where F_{obs} and F_{calc} are the observed and calculated

structure factor amplitudes.
[c] R_{free} was calculated using 5% of reflections not used during refinement.
Values in parentheses represent data in highest resolution shell.

S5. Device Fabrication

The microfluidic device used for kinetic optimization of protein crystallization and in situ diffraction studies is shown in figure S3.

Devices were fabricated using the technique of Multilayer Soft Lithography by consecutive replica molding of planar elastomer structures from microfabricated molds and bonding [13,14].

1. Mold Fabrication. Three molds used for replica micro-molding of the flow structure, control structure and fluid reservoirs were fabricated on 3" silicon wafers using standard photolithography procedures.

Reservoir molds were fabricated having circular patterns for alignment and punching of osmotic bath reservoirs as described in the MSL fabrication protocol below. Details of photoresist processing are provided below.

I. Reservoir Molds

Spin SU8 2025:	3000 rpm x 45 s / 15 second ramp up film thickness = 13 microns
Pre-Exposure Bake:	contact bake hotplate 1 min x 65 C / 5 min x 95 C
Expose Wafer:	define reservoirs 25 s at 7 mW/cm^2
Post-Exposure Bake:	1 min x 65 C / 5 min x 95 C
Develop:	100 % Shipley Nanodeveloper rinse with fresh developer dry under nitrogen

Multilevel flow molds defining the FID reactors and connecting channels were fabricated using a two-step lithography process. 16 micron high flow channels were first patterned using a positive resist, reflowed to create a rounded flow-channel cross-section, and hard-baked to withstand further processing. A 150 micron thick layer of negative resist was then applied over this structure and patterned to form the reaction chambers. Details of photoresist processing are provided below.

II. Flow Mold

Priming:	HDMS vapor 1 min in tuperware container (STP)
Spin 5740:	900 rpm x 50 s / 5 s ramp Film thickness = 16 microns
Soft Bake:	contact bake hotplate 110 C x 100 s
Expose Wafer:	define channel structure 70 at 7 mW/cm^2
Develop:	7:1 dilution of Shipley 2401 developer rinse DI H_2O dry under nitrogen
Reflow:	contact hotplate 115 C x 25 min
Hard Bake:	in oven ramp 120 C to 180 C hold 1 hr ramp 180 C to 120 C
Spin SU8 100:	1500 rpm x 60 s / 15 s ramp Film thickness = 150 microns sit for 15 minutes on flat level surface
Pre-Exposure Bake:	contact bake on level hotplate 5 min x 65 C / 30 min x 95 C / 1 min 65 C cool to room temperature
Expose Wafer:	define microwells and high i/o 130 s at 7 mW/cm^2
Post-Exposure Bake:	2 min x 65 C / 12 min x 95 C / 1 min x 65 C
Develop:	100 % Shipley Nanodeveloper rinse with fresh developer dry under nitrogen

Control molds defining the valve structures were fabricated from a single 25 micron thick layer of negative photoresist as described below.

III. Control Mold

Spin SU8 2025:	3000 rpm x 45 s / 15 second ramp up film thickness = 13 microns
Pre-Exposure Bake:	contact bake hotplate 1 min x 65 C / 5 min x 95 C
Expose Wafer:	define control structure 25 s at 7 mW/cm^2
Post-Exposure Bake:	1 min x 65 C / 5 min x 95 C
Develop:	100 % Shipley Nanodeveloper rinse with fresh developer dry under nitrogen
Hard Bake:	contact hotplate 150 C x 60 min

MSL Fabrication

Replica molding and bonding steps are detailed below.

Priming: (STP)	all molds were treated with Trimethylchlorosilane (TMCS) vapor for 5 min
Cast Reservoir Layer:	36 grams of silicone elastomer (GE 615 RTV) was combinded at a 5:1 ratio (36 g A: 7 g B) and poured onto reservoir mold (thickness ~ 7.5 mm)
Degas Reservoir Layer:	Reservoir mold was subject to vacuum (~90 Torr) for 30 minutes
Spin Flow Layer 1:	A 180 micron thick layer of 5:1 (A:B) GE 615 RTV was applied to the flow mold by spin coating at 350 rpm for 60 s.
Degas Flow Layer:	Reservoir mold was subject to vacuum (~90 Torr) for 10 minutes
Spin Control Layer:	A 28 micron thick layer of 20:1 (A: B) GE 615 RTV was applied to the control mold by spin coating at 1800 rpm for 60 s.

Spin Blank Layer:	A 30 micron thick layer of 20:1 (A: B) GE 615 RTV was applied to an unpatterned 3" silicon wafer by spin coating at 2000 rpm for 60 s.
1st Cure Reservoir Layer:	The reservoir mold was cured at 80 C for 80 minutes in a convection oven
1st Cure Flow Layer:	The flow mold was cured at 80 C for 60 minutes in a convection oven
Spin Flow Layer 2:	A 30 micron thick layer of 20:1 (A: B) GE 615 RTV was applied to the control mold by spin coating at 2000 rpm for 60 s.
2nd Cure Control Layer:	The flow mold was cured at 80 C for 20 minutes in a convection oven
Punching Reservoirs:	The reservoir layer was released from the mold and reservoirs were punched using a 3/8" punch tool.
Reservoir/Flow Bonding:	The reservoir layer was aligned to the flow layer and baked at 80 C for 60 minutes to bond the layers.
1st Cure Control Layer:	The control layer was cured at 80 C for 40 minutes in a convection oven.
Control/Flow Bonding:	The bonded flow and reservoir layers were peeled from the flow mold and aligned to the control layer. The three layers were then cured at 80 C for 70 minutes to bond the flow and control layers.
1st Cure Blank Layer:	The blank layer was cured at 80 C for 40 minutes in a convection oven.
Puncing I/O Ports:	The bonded control, flow, and reservoir layers were peeled from the control mold and input flow and control ports were punched.
Blank/Control Bonding:	The bonded layers were placed on the blank layer and cured at 80 C for 12 hours to seal the device.
Dicing:	The finished device was peeled from the unpatterned silicon wafer, cut to size, and mounted on a microscope slide.

Supplementary Figures

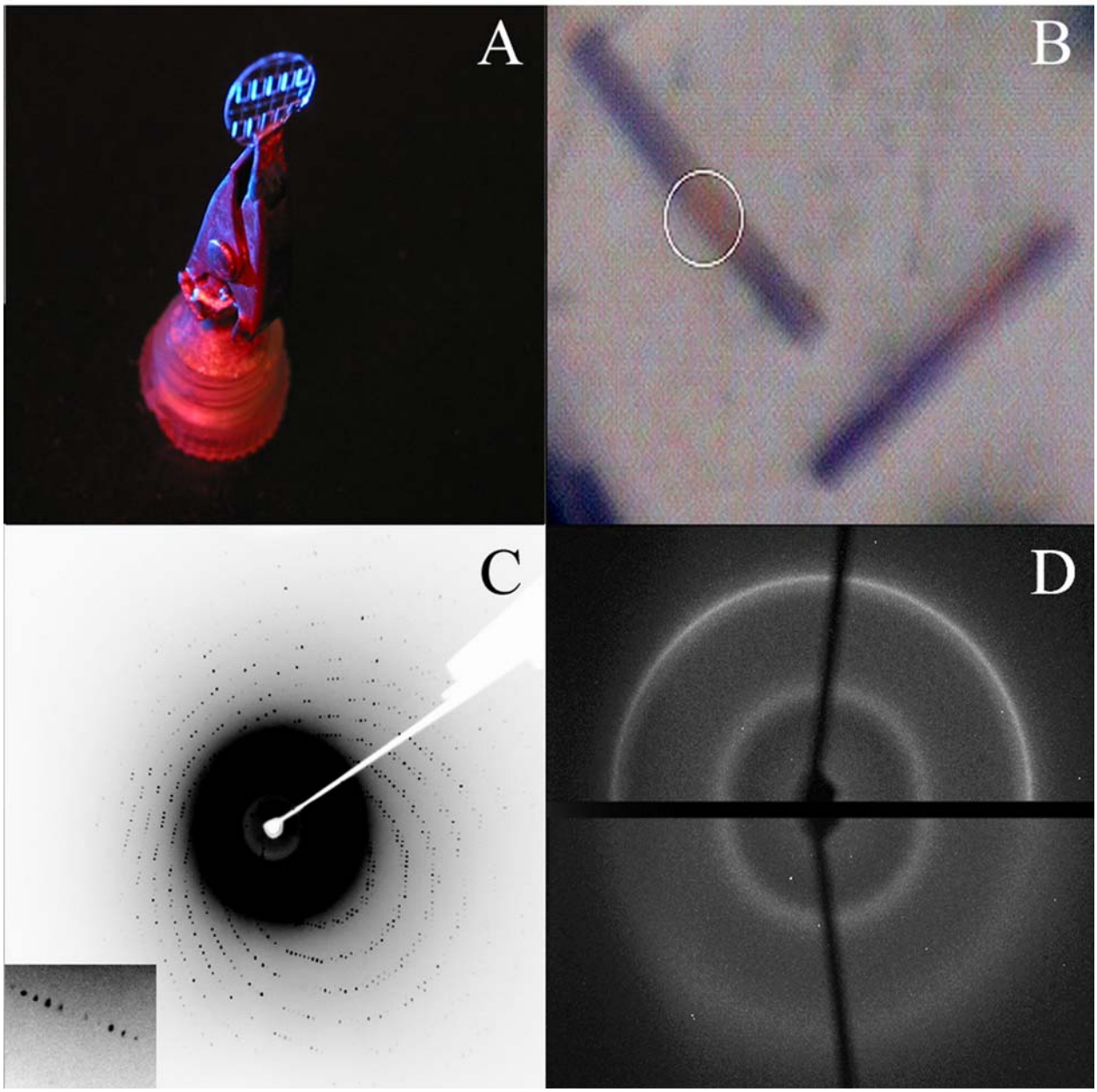

Figure S1. In situ diffraction studies of crystals grown in semi-permeable elastomer membranes. **a.** Membrane disk of PDMS mounted on a modified crystal cap *in situ*. **b.** Optical micrograph showing the alignment of crystals of BOP for x-ray analysis. The

crystal on the right is being irradiated with a 30 μm diameter x-ray beam focused at the white circle. Proper alignment of the beam with the crystal is apparent from the localized discoloration due to x-ray photo-bleaching. **c.** High resolution diffraction pattern of a lysozyme crystal mounted in a PDMS membrane. Image was taken on a home source (R-AXIS IV; Rigaku) with 1° oscillation and 15 minute exposure using a copper anode generator (λ = 1.542 Å). Inset shows clear reflections at 1.6 Å which was the limit of the detector. **d.** Diffraction patterns of PDMS membranes showing the freezing transition from microcrystalline ice formation at 28 % v/v glycerol (top) to amorphous glass at 30% v/v glycerol (bottom). The sharp ring at approximately 3.7 Å indicates microcrystalline ice formation in the top image. A diffuse powder diffraction ring from the PDMS membrane is visible at approximately 7 Å in both images. Images were taken as in (c) with 2 minute exposure.

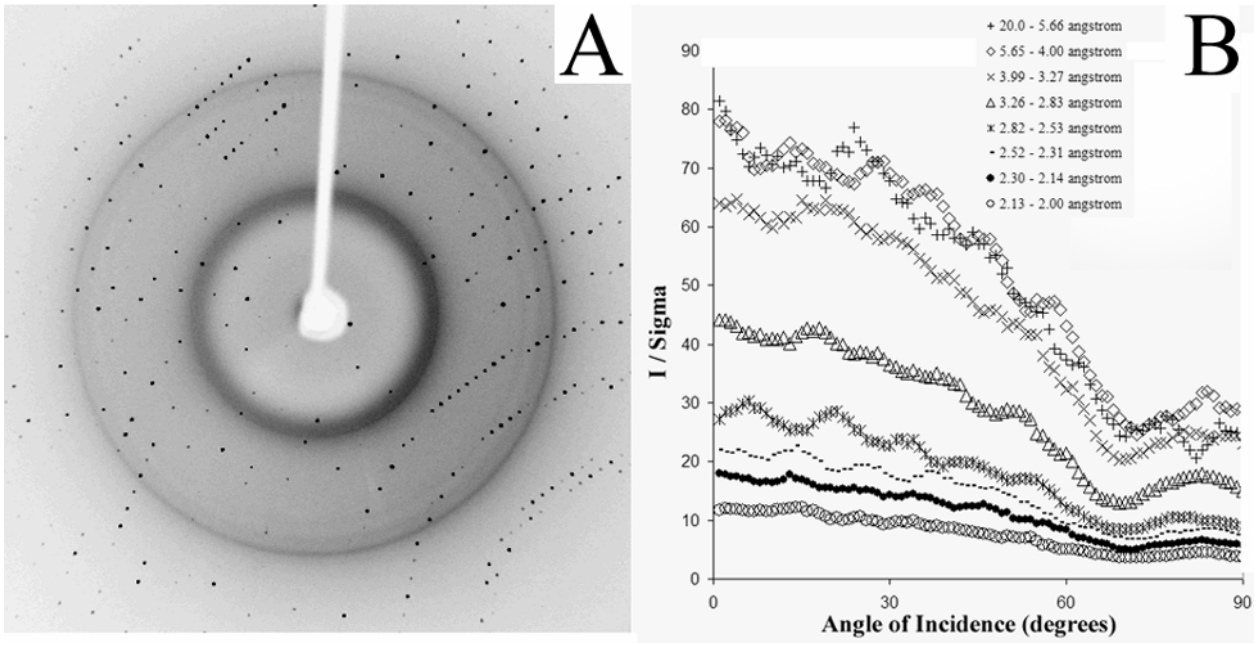

Figure S2. Anisotropy in X-ray scatter and absorption. **a.** Home source (R-AXIS IV; Rigaku) oscillation image of diffraction pattern with x-rays incident 45° from normal showing anisotropic background scatter and reflection intensities. Image was taken at 100 K with 1° oscillation and 15 minute exposure at a detector distance of 250 mm. **b.** Plot of I/σ as a function of angle of x-ray incidence from normal to membrane for resolution bands from 20 Å to 2 Å. Each point represents a 5° moving average of I/σ values determined from 1° oscillations. Data were collected on a home source (R-AXIS IV; Rigaku) with 20 minute exposures and detector distance of 150 mm from a single thaumatin crystal.

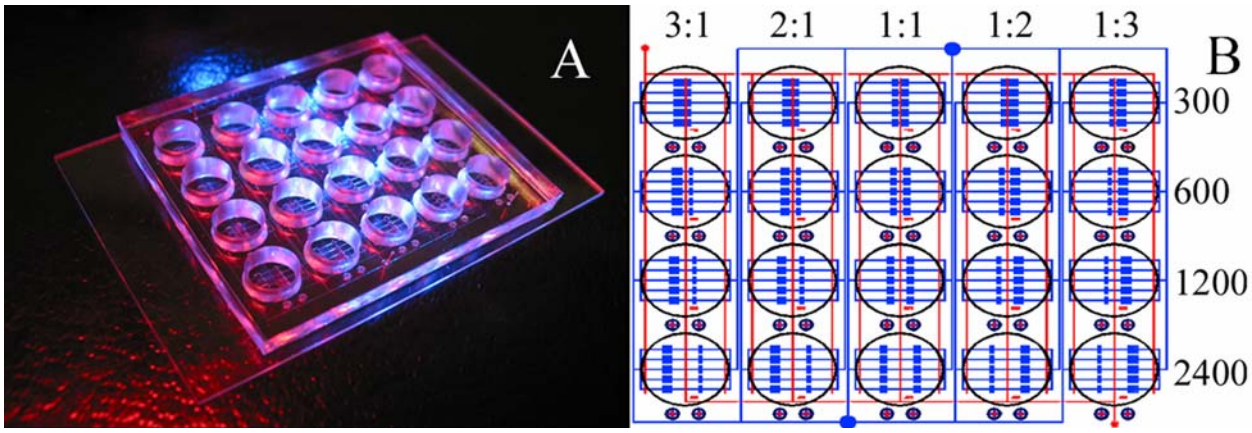

Figure S3. Microfluidic device for protein crystal growth by combined free interface and membrane-mediated vapor diffusion in semi-permeable elastomer membranes. **a.** Photograph of microfluidic device mounted on a 2" x 3 ½" microscope slide showing the 3/8" circular wells that comprise 20 independent reaction sites. **b.** Schematic showing layout of device channels (blue) and valve structures (red). Two reagent inlets (blue dots) permit loading of a concentrated protein solution and a single crystallization solution. A microfluidic channel structure simultaneously distributes each solution to distinct reaction

sites (black circles) each containing five separate FID reactors. The entire array of reaction sites consists of five columns that contain protein solution to crystallization solution mixing ratios of 3:1, 2:1, 1:1, 1:2, and 1:3, and four rows with different diffusion channel lengths (300, 600, 1200, and 2400 μm).

(1) MacDowell, A. A.; Celestre, R. S.; Howells, M.; McKinney, W.; Krupnick, J.; Cambie, D.; Domning, E. E.; Duarte, R. M.; Kelez, N.; Plate, D. W.; Cork, C. W.; Earnest, T. N.; Dickert, J.; Meigs, G.; Ralston, C.; Holton, J. M.; Alber, T.; Berger, J. M.; Agard, D. A.; Padmore, H. A. *Journal of Synchrotron Radiation* **2004**, *11*, 447-455.

(2) Holton, J.; Alber, T. *Proc. Natl. Acad. Sci. U. S. A.* **2004**, *101*, 1537-1542.

(3) Otwinowski, Z.; Minor, W. In *Macromolecular Crystallography, Pt A*, 1997; Vol. 276, pp 307-326.

(4) Storoni, L. C.; McCoy, A. J.; Read, R. J. *Acta Crystallographica Section D-Biological Crystallography* **2004**, *60*, 432-438.

(5) Read, R. J. *Acta Crystallographica Section D-Biological Crystallography* **2001**, *57*, 1373-1382.

(6) Wilson, K. P.; Malcolm, B. A.; Matthews, B. W. *Journal of Biological Chemistry* **1992**, *267*, 10842-10849.

(7) Sauter, C.; Lorber, B.; Giege, R. *Proteins-Structure Function and Genetics* **2002**, *48*, 146-150.

(8) Fita, I.; Rossmann, M. G. *Proc. Natl. Acad. Sci. U. S. A.* **1985**, *82*, 1604-1608.

(9) Dauter, Z.; Terry, H.; Witzel, H.; Wilson, K. S. *Acta Crystallographica Section B-Structural Science* **1990**, *46*, 833-841.

(10) Perrakis, A.; Harkiolaki, M.; Wilson, K. S.; Lamzin, V. S. *Acta Crystallographica Section D-Biological Crystallography* **2001**, *57*, 1445-1450.

(11) Murshudov, G. N.; Vagin, A. A.; Dodson, E. J. *Acta Crystallographica Section D-Biological Crystallography* **1997**, *53*, 240-255.

(12) Jones, T. A.; Zou, J. Y.; Cowan, S. W.; Kjeldgaard, M. *Acta Crystallographica Section A* **1991**, *47*, 110-119.

(13) Unger, M. A.; Chou, H. P.; Thorsen, T.; Scherer, A.; Quake, S. R. *Science* **2000**, *288*, 113-116.

(14) Thorsen, T.; Maerkl, S. J.; Quake, S. R. *Science* **2002**, *298*.